Short-Duration Doppler Spectrogram for Person Recognition with a Handheld Radar

Michael Ulrich and Bin Yang
Institute of Signal Processing and System Theory, University of Stuttgart
Pfaffenwaldring 47, 70550 Stuttgart, Germany
Email: {michael.ulrich, bin.yang}@iss.uni-stuttgart.de

***Abstract*—This paper examines the classification of walking, standing and mirrored persons based on radar micro-Doppler (m-D) measurements to resolve ambiguities in thermal infrared (TIR) mirror images in firefighting. If the walking or standing person is observed directly, its m-D is measured. In the case of a person mirrored on a reflecting object, only the m-D of the reflecting object is measured. Their spectrogram is differentiable which enables a classification. One difficulty is the random movement of the handheld radar which leads to short observation durations and Doppler blurring. A classification based on short spectrograms is proposed, where the influence of the short-time Fourier transform window length is investigated. Furthermore, a regularization is proposed to improve the classifier interpretability for this safety application.**

I. Introduction

This paper investigates the person recognition using a handheld radar system. Our application is a handheld thermal infrared (TIR) camera for firefighters, which is enhanced by a radar sensor. The main purpose of the radar sensor is localization. However, this paper examines the radar target classification in firefighting. The TIR camera as well as the radar are able to measure through smoke. In the TIR image, reflections of firefighters occur on flat surfaces (e.g. on glass, metal or painted surfaces) which are often mistaken for a person to be rescued, see Fig. 2. This has to be resolved.

The Doppler of a radar signal is a frequency shift due to the relative radial velocity between the radar and a target. If the target consists of multiple scatterers such as limbs of a person, their differences in velocity lead to multiple Doppler frequencies, which are termed micro-Doppler (m-D). The m-D often takes the form of sidelobes in the Doppler spectrum near the main Doppler frequency. Their shape is usually characteristic for the target type and is hence utilized for target classification.

In this paper, the radar sensor is used to classify persons, which is a useful decision support for firefighters. The terms "real" and "mirrored" person are used with respect to the TIR image, i.e. a real person is observed directly, whereas a reflection on a flat surface is a mirrored person. A walking person and a standing person with subtle movements of body parts show sidelobes in the m-D. In contrast, a mirroring object has no moving parts at all and a mirrored person (e.g. a mirrored firefighter) exhibits a single significant peak in the Doppler spectrum. The contributions of this paper are:

- The first approach which allows a classification of walking, standing and mirrored persons with a moving (handheld) radar.
- A radar signal processing chain to extract spectrograms, while simultaneously permitting localization.
- An improved choice of the spectrogram window length to make subtle movements of standing persons observable.
- A novel regularization for the training of the classifier to improve the interpretability of the learned features.

This paper is organized as follows: The next Sec. II revises previous works. Sec. III discusses the signal processing and the trade-off between Doppler resolution and blurring. The person classification is explained in Sec. IV. Experiments with real measurements are shown in Sec. V and Sec. VI concludes this paper.

II. Previous works

The m-D is commonly used to classify radar targets such as humans [1]. Well-known applications are the elderly fall detection [2] or the classification of different human activities. Human activities are classified with high accuracy [3], through a wall [4], in an environment with strong clutter [5] or in multi-target scenarios [6]. In [7], the wavelet transform was used instead of the spectrogram to improve the temporal resolution. 2-D convolutional neural networks (CNNs) were applied to classify m-D spectrograms, which are treated similar to images in [8], [9], [10], [11].

[2]-[10] require an observation length of several seconds, which is not possible in firefighting. Furthermore, they use an unmodulated continuous wave radar, which is unable of localizing targets because range estimation is impossible. Moreover, [2]-[11] use a stationary radar and are hence unsuitable in our handheld scenario.

Another well-known application is object classification for automotive, where persons, bikes, cars, trucks and other objects are distinguished [12], [13], [14]. In this application, only short radar measurements are evaluated and the shape of the peaks in the Doppler spectrum is used for classification. The temporal behavior is not utilized at all. To improve the visibility of person m-D, [15] suggests to increase the radar carrier frequency and [16] suggests to increase the measurement duration. [17] gives an overview of alternative measurement methods, e.g. using a radar interferometer for measuring radial velocities or a passive radiometer.

The modulation used in these automotive applications is able to combine localization and classification. However, only the m-D spectrum is used rather than the spectrogram. The spectrum is calculated over a few milliseconds, leading to a bad Doppler resolution. Consequently, only persons with strong movements (e.g. walking) can be classified and standing persons are unrecognizable.

In contrast, the approach of this paper combines the benefits of the automotive radar modulation for localization and the spectrogram-based methods for recognition of walking, standing or mirrored persons using a handheld radar.

ISBN 978-90-827970-1-5

Modulation parameter	value
Chirp bandwidth B	3GHz
Carrier frequency f	94GHz
Number of samples N_f	1000
Chirp interval T_p	200μs
Number of chirps N_p	2048 (0.41s)

Fig. 1: Photograph of the handheld radar system and summary of the modulation parameters of this work. Further details are given in [18].

III. Radar signal processing

A. Radar system

The radar system of [18] is used in this work, see Fig. 1. It uses the chirp sequence radar waveform [19], [20], [21]:

$$x(n_\mathrm{f}, n_\mathrm{p}) = \sum_{k=1}^{K} A_k \exp\left(2\pi j \left(\frac{2Br_k}{Tc} T_\mathrm{f} n_\mathrm{f} + \frac{2fv_k}{c} T_\mathrm{p} n_\mathrm{p}\right)\right) + n(n_\mathrm{f}, n_\mathrm{p}) \quad (1)$$

x is the measured signal with fast- and slow time sample index $n_\mathrm{f} \in \{1, ..., N_\mathrm{f}\}$ and $n_\mathrm{p} \in \{1, ..., N_\mathrm{p}\}$. T_f and T_p are the sampling and pulse repetition interval, respectively. T is the pulse duration (usually $T \leq T_\mathrm{p}$), f is the carrier frequency, c the propagation speed of the electromagnetic wave, and B is the bandwidth. The signal is considered as a superposition of K scattering points (from a single or multiple objects), where A_k, r_k, and v_k are the (complex) amplitude, range and radial velocity of the k-th scatterer. The velocity differences of multiple scatterers of a single object correspond to the m-D. Fig. 1 summarize the radar modulation settings. The modulation design is according to the requirements of the radar localization task in firefighting, except for the total number of recorded chirps ($N_\mathrm{p} = 2048$), which is significantly larger than usual. With such a high measurement duration, the Doppler resolution is greatly improved. However, an application of the two-dimensional DFT to obtain the range-Doppler spectrum is not possible because of Doppler blurring (non-stationary Doppler, cf. Sec. III-B).

Instead, the following signal processing is proposed: After calibration and windowing, a one-dimensional discrete Fourier transform (DFT) is applied row-wise to convert the fast-time samples into a range spectrum, see the range-slow-time matrix in Fig. 3. Then, an incoherent integration (sum of absolute values) of the range spectrum is performed over all N_p chirps and targets are detected using a CFAR detector in range direction. For each detected target at a range bin, the corresponding column of the range-slow time matrix forms the so-called target signal (N_p samples), see Fig. 3. The spectrogram of each target signal is used for classification in the sequel.

In addition to the m-D, also the micro-ranges (m-r, characteristic shape of radar targets in range direction) could be used to improve classification. However, this paper examines a classification on m-D alone to focus on the trade-off of blurring and Doppler resolution. An extension to a classification using both m-D and m-r is straightforward.

B. Spectrogram and Doppler blurring

For the spectrogram of the target signal, the choice of the short-time Fourier transform (STFT) window length N_w ($N_\mathrm{w} \leq N_\mathrm{p}$) is crucial. The spectrogram has the size $N_\mathrm{w} \times N_\mathrm{t}$,

(a) Infrared image of a real person

(b) Infrared image of a person mirrored on a flat surface.

Fig. 2: Infrared image of a real person and its mirror image on a flat surface (whiteboard) are difficult to distinguish for firefighters.

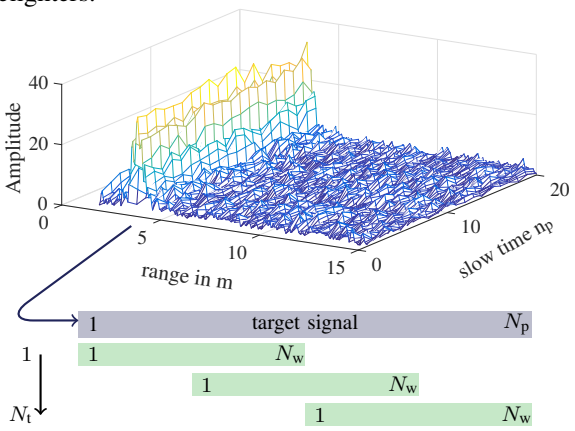

Fig. 3: A target signal is extracted from the range-slow time matrix for each detected target. It is then divided into N_t overlapping windows to calculate the spectrogram.

where N_t is the number of time samples in the spectrogram. If N_w is large, the Doppler resolution is high, but Doppler blurring can occur if the Doppler and m-D are changing over this window interval. A spectrogram with a small N_w is free of Doppler blurring, but the Doppler resolution is low, which makes classification difficult. In this paper, 50% overlap of the STFT windows is chosen, see Fig. 3.

After calculating the spectrogram of a target signal, an incoherent integration over N_t windows and the application of a CFAR detector yields the main frequency peak at the target Doppler. To take the ego-velocity of the handheld radar into account, the part of the spectrogram containing the target Doppler and neighboring velocity bins in a range of $\pm 0.5 \frac{\mathrm{m}}{\mathrm{s}}$ is extracted, see Fig. 4. Furthermore, the extracted spectrogram is scaled (multiplied) with the target range to the power of 4 to compensate the radar path propagation loss.

To illustrate the trade-off between Doppler resolution and blurring, Fig. 4 shows some spectrograms of the target signals of a walking, standing and mirrored person. Fig. 4 (a), (d) and (g) show the Doppler spectrogram for $N_\mathrm{w} = 256$. This is similar to the modulation of the automotive approaches in [11], [12], [13], [14]. In this case, the m-D of the standing person is hardly visible due to a low Doppler resolution and the shapes of the peaks of the standing person and mirrored person are similar. However, a walking person has a distinctive m-D. Increasing N_w to 1024, Fig. 4 (e) and (h) show that the m-D of the standing person and the mirrored person can now be distinguished due to a higher Doppler resolution. Fig. 4 (e) shows the m-D of the standing person where sidelobes

ISBN 978-90-827970-1-5

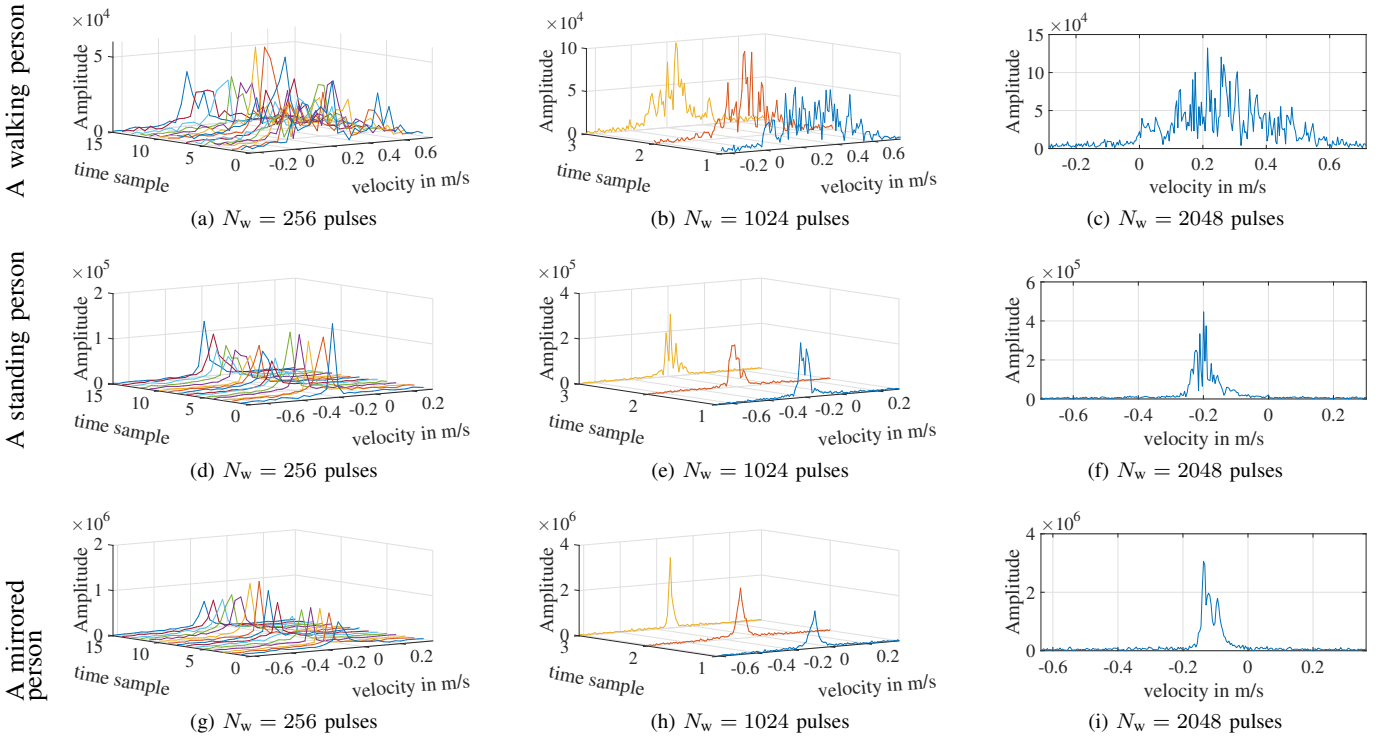

(a) $N_w = 256$ pulses (b) $N_w = 1024$ pulses (c) $N_w = 2048$ pulses

(d) $N_w = 256$ pulses (e) $N_w = 1024$ pulses (f) $N_w = 2048$ pulses

(g) $N_w = 256$ pulses (h) $N_w = 1024$ pulses (i) $N_w = 2048$ pulses

Fig. 4: m-D spectrograms for a walking, standing and mirrored person for different STFT window lengths. For $N_w = 1024$ the standing person and the mirrored person are clearly distinguishable. All data in (a)-(c), (d)-(f) and (g)-(i) stem from the same target signals respectively. The offset of the velocity axis is due to the extraction of the target peaks and neighboring velocity bins to compensate ego-motion of the firefighter.

next to the main peak are visible. In contrast, the m-D of the mirrored person in Fig. 4 (h) contains only a single peak because of the block motion of the mirrored person. However, a further increment of N_w to 2048 in Fig. 4 (c), (f) and (h) with $N_w = N_p$ and $N_t = 1$ leads to Doppler blurring. Both Doppler spectra of the standing person and mirrored person contain sidelobes next to the main peak.

These m-D sidelobes are due to the body motion (a person naturally does not stand completely still). The m-D of still persons (e.g. breathing or heart beat) was indistinguishable from the handheld motion blurring in our experiments.

IV. Classification of Persons and Objects

A. Architecture

In firefighting, real and mirrored persons are to be distinguished by the classifier. This is a binary classification problem. However, we found that it is better to perform a 3-class classification into walking, standing and mirrored person because of a high confusion between standing and mirrored persons. Hence, a 3-class classifier is trained and the results of walking and standing persons are subsequently merged to the person class. The spectrograms generated in Sec. III (Fig. 4) are used as input to the classifier.

In this paper, we use neural networks (NN) for classification. Spectrograms can be treated as images and fed to a NN with 2-dimensional input (2-D NN), similar to [8], [9], [11], [10]. A single classification result is obtained for each spectrogram.

Alternatively, a 1-dimensional input can be used to classify the N_t different m-D spectra of a spectrogram separately (1-D NN). Then the classification results of the individual m-D spectra are combined to make a decision for the whole spectrogram. This paper uses a majority vote of the N_t classification results for the final decision.

This work uses NN with 3 fully-connected layers. While convolutional layers (CNNs) improved the classification in previous literature, experiments showed that this is not the case in this application. The reason is a different preprocessing of the data. The convolutional and pooling layers in [8], [9], [11], [10] are necessary to obtain an invariance of the target peak position (absolute velocity) in the spectrogram. In contrast, the spectrograms of this work are already centered around the main peak by the preprocessing.

The spectrogram bins of the input layer were normalized to zero mean and unit variance independently. The first two layers (relu-activation) perform feature extraction and the last layer (softmax activation) performs classification. Deeper architectures did not lead to an improved classification in our experiments with the given dataset.

B. Regularization

An unregularized training (using only the categorical cross-entropy as training loss) leads to network weights which are difficult to interpret. This is problematic in our safety critical application. The first dense layer is expected to extract features. The second dense layer is expected to combine those features and the last dense layer performs classification. To realize this intuition in the given network, different regulizers are proposed.

ISBN 978-90-827970-1-5 © EURASIP 2018

[14] uses hand-crafted filters for the m-D as features, which are easily interpretable. In this work, such interpretable features are learned from the data. In the 1-D case, the kernel weights reflect which m-D components are used for classification (features). The intention is that neighboring m-D cells should have similar weights. The motivation for this is that contiguous regions in the m-D spectra can be associated with particular sidelobes. These sidelobes can have a physical or anatomical interpretation. Examples will be given in Sec. V. Furthermore, such kernels are more robust to slight variations of the m-D than arbitrary weights. Such continuous weights can be achieved by penalizing the sum of absolute or squared differences of the weight matrix entries:

$$r_{l1} = \lambda_{1,1} \sum_{n_1=1}^{N_1} \sum_{n_0=1}^{N_0-1} |[\mathbf{W}_1]_{(n_1,n_0)} - [\mathbf{W}_1]_{(n_1,n_0+1)}| \quad (2)$$

$$r_{l2} = \lambda_{1,2} \sum_{n_1=1}^{N_1} \sum_{n_0=1}^{N_0-1} |[\mathbf{W}_1]_{(n_1,n_0)} - [\mathbf{W}_1]_{(n_1,n_0+1)}|^2 \quad (3)$$

where $[\mathbf{W}_1]_{(n_1,n_0)}$ is the (n_1,n_0)-th entry of the weight matrix of the first dense layer $\mathbf{W}_1$. n_0, n_1 are indices for the input layer and first dense layer neurons, ranging from 1 to the number of input neurons N_0 and the number of neurons in the first dense layer N_1, respectively. r_{l1} in Eq. 2 is an l1-regularizer (l1-r) on the first weight matrix differences and r_{l2} in Eq. 3 is an l2-regularizer (l2-r) on the same. The effect of the norm (l1 or l2) is examined in Sec. V. $\lambda_{1,1}$ and $\lambda_{1,2}$ are the weighting factor for the regularization of the first layer. For efficient training, the sums in Eq. 2 and 3 can be implemented as matrix operations.

In the second layer, a l1-regularization on all elements of the weight matrix $\lambda_2||\mathbf{W}_2||_1$ is applied. The motivation for this is to ensure that the second layer only combines features from the first dense layer. Otherwise, features could implicitly be generated in the second layer and the regularization of the first layer would be bypassed. The classification layer is not regularized.

V. Experiments

This section compares the classification approaches discussed in Sec. IV. A dataset was created by measuring multiple indoor scenarios with different persons, rooms and movements of the radar. To increase the number of samples, a flipped (along the m-D axis) version of all spectrograms is also added to the dataset (data augmentation). In the dataset the numbers of samples of walking and standing persons are equal and the number of mirrored persons is twice as high to obtain a balanced dataset with respect to the original binary problem. The training dataset consists of 1904 samples (476 standing persons, 476 walking persons and 952 mirroring indoor objects, such as walls, windows or furniture) and the test dataset consists of 228 samples (57 standing, 57 walking, 114 mirrored).

This paper uses real radar measurements. Care has to be taken when dividing the data into training and test datasets. All spectrograms from one measurement scenario (room, person) are either in the training or test dataset to avoid overfitting. Each sample consists of $N_\mathrm{p} = 2048$ chirps, which correspond to a measurement duration of 0.41s. The network consists of $N_1 = 64$ and $N_2 = 16$ hidden neurons and was trained using

TABLE I: Average test accuracy and BER for standing, walking and mirrored persons

N_w	classifier	α_m	α_w	α_s	BER
256	1-D NN	0.789	1	0.895	0.131
	1-D NN l1-r	0.772	1	0.945	0.127
	1-D NN l2-r	0.789	1	0.930	0.123
	2-D NN	0.807	1	0.667	0.180
341	1-D NN	0.789	1	0.947	0.118
	1-D NN l1-r	0.789	0.982	0.947	0.123
	1-D NN l2-r	0.789	1	0.947	0.118
	2-D NN	0.825	1	0.702	0.162
512	1-D NN	0.789	0.982	0.982	0.114
	1-D NN l1-r	0.771	0.982	0.965	0.127
	1-D NN l2-r	0.781	0.982	0.965	0.123
	2-D NN	0.807	0.947	0.930	0.127
682	1-D NN	0.789	1	0.982	0.109
	1-D NN l1-r	0.781	0.982	0.982	0.118
	1-D NN l2-r	0.789	1	0.982	0.109
	2-D NN	0.798	1	0.737	0.167
1024	1-D NN	0.754	0.965	0.982	0.135
	1-D NN l1-r	0.789	0.965	0.982	0.118
	1-D NN l2-r	0.781	0.965	0.965	0.127
	2-D NN	0.77	1	0.75	0.175
2048	1-D NN	0.746	1	0.982	0.131
	1-D NN l1-r	0.754	0.982	0.982	0.131
	1-D NN l2-r	0.754	0.982	0.982	0.131

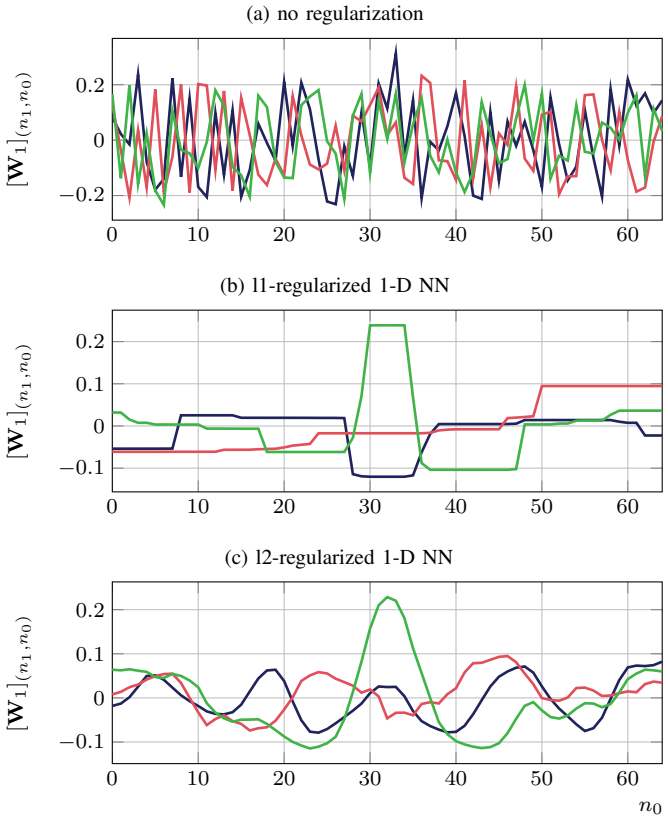

Fig. 5: Examples of the learned Kernels of the first layer (1D NN) of $N_\mathrm{w} = 512$. Without regularization, the learned weights are difficult to interpret. In contrast, features such as mainlobe, sidelobes or their superpositions are visible with the proposed regularization. l1-regularization leads to regions of constant weights with sharp boundaries, while l2-regularization leads to smooth kernels.

ISBN 978-90-827970-1-5 © EURASIP 2018

Keras. r_{l1} or r_{l2} are weighted with $\lambda_{1,1} = 0.003$ and $\lambda_{1,2} = 0.01$, respectively and $\lambda_2 = 10^{-6}$, cf. Sec. IV-B.

In the experiments of this paper, different window lengths of $N_\mathrm{w} \in \{2048, 1024, 682, 512, 341, 256\}$ are compared. The accuracy (rate of the correctly classified samples and the number of all samples of a class) of walking persons α_w, standing persons α_s and mirrored persons α_m as well as the balanced error rate (BER, rate of all false classifications and all test samples) are used for evaluation. For the application of this paper, a distinction of walking and standing persons is insignificant, hence only the confusion of real and mirrored persons is analyzed.

The results are shown in Tab I. Walking persons are mostly classified correctly. In contrast, mirrored persons are sometimes confused as standing persons, due to their similar m-D. The 2-D NN approach (similar to [11]) behaves reasonable, but its performance is worse than a separate classification of all m-D and subsequent combination (the 1-D NN proposed in this paper). The reason is that for short spectrograms of 0.41s, the temporal characteristic is not very informative. The 1-D NN converge better than the 2-D NN because they have less training parameters and hence utilize the limited dataset better. The 1-D NN are trained on $1904 \cdot N_\mathrm{t}$ samples, while only 1904 samples are available for the 2-D NN.

The best classification (based on BER) is obtained for the 1-D NN with $N_\mathrm{w} = 682$ (corresponding to 0.136s). Larger N_w result in Doppler blurring due to the handheld motion and smaller N_w reduce the Doppler resolution, as discussed in Sec. III-B. Although the optimality of $N_\mathrm{w} = 682$ can only be demonstrated for one particular application, this result indicates that window durations in the order of 0.136s would also improve the performance in other applications. This is consistent with the result of [16].

Examples of the learned kernels of the first dense layer are depicted in Fig. 5. Fig. 5(a) shows the kernel weights when no regularization was applied during training. In this case, no characteristic pattern can be observed. In contrast, the l1-r and l2-r in Fig. 5(b) and (c) clearly reveal the learned features. The green curves can be interpreted as a feature for the mainlobe, while the red curves have high amplitudes at some sidelobes. The blue curve in Fig. 5(c) has a periodic structure, which might resemble a feature for swinging limbs (e.g. the hand/foot moves twice as fast as the elbow/knee). Interestingly, the proposed regularization has only a minor influence on the performance of the 1-D NN. The l2-r achieves the same result as the unregularized 1-D NN for $N_\mathrm{w} = 682$, while the l1-r performs slightly worse. Hence, generating interpretable kernels comes at almost no performance loss, which is an advantage in this safety application.

VI. Conclusion

This paper examines the m-D based classification of real and mirrored persons using a handheld radar for firefighting. For each range target, the slow time signal is extracted and its Doppler spectrum or spectrogram is used for a successful classification using 1-D or 2-D NNs. A STFT window length of approximately 0.136s performed best. Furthermore, regularization on the NN weight matrices is investigated to improve the interpretability of what the NN learned. A l2-regularization of the first dense layer combined with a l1-regularization of the weights of the following layer leads to interpretable features without a loss of classification performance.

Acknowledgment

This work was supported by the German Federal Ministry of Education and Research, Grant No. 13N13480, project "FeuerWeRR".

References

[1] V.C. Chen, "Analysis of radar micro-Doppler with time-frequency transform," in *Proceedings of the Tenth IEEE Workshop on Statistical Signal and Array Processing*, 2000.

[2] Moeness G. Amin, Yimin D. Zhang, Fauzia Ahmad, and K.C. Dominic Ho, "Radar signal processing for elderly fall detection: The future for in-home monitoring," *IEEE Signal Processing Magazine*, vol. 33, no. 2, pp. 71 – 80, 2016.

[3] Cesur Karabacak, Sevgi Z. Gurbuz, Ali C. Gurbuz, Mehmet B. Guldogan, Gustaf Hendeby, and Fredrik Gustafsson, "Knowledge exploitation for human micro-Doppler classification," *IEEE Geoscience and Remote Sensing Letters*, vol. 12, no. 10, pp. 2125 – 2129, 2015.

[4] Youngwook Kim and Hao Ling, "Human activity classification based on micro-Doppler signatures using a support vector machine," *IEEE Transactions on Geoscience and Remote Sensing*, vol. 47, no. 5, pp. 1328 – 1337, 2009.

[5] Jihoon Kwon and Nojun Kwak, "Human detection by neural networks using a low-cost short-range Doppler radar sensor," in *2017 IEEE Radar Conference*, 2017.

[6] Thomas Wagner, Reinhard Feger, and Andreas Stelzer, "Radar signal processing for jointly estimating tracks and micro-Doppler signatures," *IEEE Access*, vol. 5, pp. 1220 – 1238, 2017.

[7] T. Thayaparan, S. Abrol, E. Riseborough, L. Stankovic, D. Lamothe, and G. Duff, "Analysis of radar micro-Doppler signatures from experimental helicopter and human data," *IET Radar, Sonar & Navigation*, vol. 1, no. 4, pp. 289 – 299, 2007.

[8] Youngwook Kim and Taesup Moon, "Human detection and activity classification based on micro-Doppler signatures using deep convolutional neural networks," *IEEE Geoscience and Remote Sensing Letters*, vol. 13, no. 1, pp. 8 – 12, 2016.

[9] R.P. Trommel, R.I.A. Harmanny, L. Cifola, and J.N. Driessen, "Multi-target human gait classification using deep convolutional neural networks on micro-Doppler spectrograms," in *European Radar Conference*, 2016.

[10] Youngwook Kim, Jinhee Park, and Taesup Moon, "Classification of micro-Doppler signatures of human aquatic activity through simulation and measurement using transferred learning," in *Radar Sensor Technology*, 2017.

[11] Karthick N. Parashar, Meshia Cdric Oveneke, Maxim Rykunov, Hichem Sahli, and Andr Bourdoux, "Micro-Doppler feature extraction using convolutional auto-encoders for low latency target classification," in *IEEE Radar Conference*, 2017.

[12] Hermann Rohling, Steffen Heuel, and Henning Ritter, "Pedestrian detection procedure integrated into an 24 GHz automotive radar," in *IEEE Radar Conference*, 2010.

[13] Steffen Heuel and Hermann Rohling, "Pedestrian classification in automotive radar systems," in *13th International Radar Symposium*, 2012.

[14] A. Bartsch, F. Fitzek, and R. H. Rasshofer, "Pedestrian recognition using automotive radar sensors," *Advances in Radio Science*, vol. 10, pp. 45–55, 2012.

[15] Markus Andres, Karim Ishak, Wolfgang Menzel, and Hans-Ludwig Bloecher, "Extraction of micro-Doppler signatures using automotive radar sensors," *Frequenz*, vol. 66, pp. 371377, 2012.

[16] Eugen Schubert, Frank Meinl, Martin Kunert, and Wolfgang Menzel, "High resolution automotive radar measurements of vulnerable road users - pedestrians & cyclists," in *IEEE MTT-S International Conference on Microwaves for Intelligent Mobility*, 2015.

[17] Jeffrey A. Nanzer, "A review of microwave wireless techniques for human presence detection and classification," *IEEE Transactions on Microwave Theory and Techniques*, vol. 65, no. 5, pp. 1780 – 1794, 2017.

[18] Mathias Klenner, Christian Zech, Axel Hülsmann, Jutta Kühn, Michael Schlechtweg, Konstantin Hahmann, Bernhard Kleiner, Michael Ulrich, and Oliver Ambacher, "A portable w-band radar system for enhancement of infrared vision in fire fighting operations," in *SPIE 9993*, 2016.

[19] Donald E. Barrick, "FM/CW radar signal and digital processing," Tech. Rep., Nat. Ocean. Atmos. Administration, 1973.

[20] A.G. Stove, "Linear FMCW radar techniques," *IEE Proceedings F - Radar and Signal Processing*, vol. 139, no. 5, pp. 343 – 350, 1992.

[21] Peter Sorowka and Hermann Rohling, "Pedestrian classification with 24 GHz chirp sequence radar," in *16th International Radar Symposium*, 2015.